

## Article

# Identification of Soluble Degradation Products in Lithium–Sulfur and Lithium–Metal Sulfide Batteries

Fabian Horsthemke<sup>1</sup>, Christoph Peschel<sup>1</sup>, Kristina Kösters<sup>1</sup>, Sascha Nowak<sup>1</sup> , Kentaro Kuratani<sup>2</sup>, Tomonari Takeuchi<sup>2</sup>, Hitoshi Mikuriya<sup>3</sup>, Florian Schmidt<sup>4</sup>, Hikari Sakaebe<sup>2</sup> , Stefan Kaskel<sup>4</sup>, Tetsuya Osaka<sup>3,5</sup>, Martin Winter<sup>1,6</sup>, Hiroki Nara<sup>3,\*</sup> and Simon Wiemers-Meyer<sup>1,\*</sup> 

<sup>1</sup> MEET Battery Research Center, University of Münster, Corrensstraße 46, 48149 Münster, Germany; f.horsthemke@uni-muenster.de (F.H.); christoph.peschel@uni-muenster.de (C.P.); kristina.koesters@uni-muenster.de (K.K.); sascha.nowak@uni-muenster.de (S.N.); martin.winter@uni-muenster.de (M.W.)

<sup>2</sup> Research Institute of Electrochemical Energy, Department of Energy and Environment, National Institute of Advanced Industrial Science and Technology (AIST), Ikeda, Osaka 563-8577, Japan; k-kuratani@aist.go.jp (K.K.); takeuchi.tomonari@aist.go.jp (T.T.); hikari.sakaebe@aist.go.jp (H.S.)

<sup>3</sup> Research Organization for Nano & Life Innovation, Waseda University, Tokyo 162-0041, Japan; h.mikuriya@aoni.waseda.jp (H.M.); osakatets@waseda.jp (T.O.)

<sup>4</sup> Department of Chemistry, Technische Universität Dresden, 01062 Dresden, Germany; florian.schmidt@iws.fraunhofer.de (F.S.); stefan.kaskel@tu-dresden.de (S.K.)

<sup>5</sup> Faculty of Science and Engineering, Waseda University, Tokyo 169-8555, Japan

<sup>6</sup> Helmholtz Institute Münster, IEK-12, Forschungszentrum Jülich, Corrensstraße 46, 48149 Münster, Germany

\* Correspondence: h-nara@aoni.waseda.jp (H.N.); simon.wiemers-meyer@uni-muenster.de (S.W.-M.)



**Citation:** Horsthemke, F.; Peschel, C.; Kösters, K.; Nowak, S.; Kuratani, K.; Takeuchi, T.; Mikuriya, H.; Schmidt, F.; Sakaebe, H.; Kaskel, S.; et al. Identification of Soluble Degradation Products in Lithium–Sulfur and Lithium–Metal Sulfide Batteries. *Separations* **2022**, *9*, 57. <https://doi.org/10.3390/separations9030057>

Academic Editor: Mark L. Dietz

Received: 17 January 2022

Accepted: 13 February 2022

Published: 24 February 2022

**Publisher's Note:** MDPI stays neutral with regard to jurisdictional claims in published maps and institutional affiliations.



**Copyright:** © 2022 by the authors. Licensee MDPI, Basel, Switzerland. This article is an open access article distributed under the terms and conditions of the Creative Commons Attribution (CC BY) license (<https://creativecommons.org/licenses/by/4.0/>).

**Abstract:** Most commercially available lithium ion battery systems and some of their possible successors, such as lithium (metal)-sulfur batteries, rely on liquid organic electrolytes. Since the electrolyte is in contact with both the negative and the positive electrode, its electrochemical stability window is of high interest. Monitoring the electrolyte decomposition occurring at these electrodes is key to understand the influence of chemical and electrochemical reactions on cell performance and to evaluate aging mechanisms. In the context of lithium-sulfur batteries, information about the analysis of soluble species in the electrolytes—besides the well-known lithium polysulfides—is scarcely available. Here, the irreversible decomposition reactions of typically ether-based electrolytes will be addressed. Gas chromatography in combination with mass spectrometric detection is able to deliver information about volatile organic compounds. Furthermore, it is already used to investigate similar samples, such as electrolytes from other battery types, including lithium ion batteries. The method transfer from these reports and from model experiments with non-target analyses are promising tools to generate knowledge about the system and to build up suitable strategies for lithium-sulfur cell analyses. In the presented work, the aim is to identify aging products emerging in electrolytes regained from cells with sulfur-based cathodes. Higher-molecular polymerization products of ether-based electrolytes used in lithium-sulfur batteries are identified. Furthermore, the reactivity of the lithium polysulfides with carbonate-based solvents is investigated in a worst-case scenario and carbonate sulfur cross-compounds identified for target analyses. None of the target molecules are found in carbonate-based electrolytes regained from operative lithium-titanium sulfide cells, thus hinting at a new aging mechanism in these systems.

**Keywords:** batteries; lithium-sulfur batteries; LiS; lithium-metal batteries; lithium-metal sulfide batteries; electrolyte decomposition; gas chromatography; mass spectrometry; structural elucidation

## 1. Introduction

The lithium-sulfur (LiS) chemistry represents a promising alternative to state-of-the-art lithium ion battery (LIB) technology. Especially for applications demanding a high gravimetric energy density, such as aviation and space programs, LiS cells provide lightweight

energy storage [1–3]. Furthermore, the utilization of sulfur as a cathode active material (CAM) is beneficial as it is an abundant, low-cost material in comparison to more expensive transition metals used in state-of-the-art LIB cathodes [4–7].

The LiS chemistry has a variety of challenges yet to overcome. The most prominent challenge reported in the community is the prevention of the polysulfide shuttle effect leading to self-discharge and loss of active material. Moreover, standard LiS cells are not compatible with carbonate-based electrolyte systems—typically used in LIBs [8]—due to their reactivity in combination with soluble lithium polysulfides emerging during cell discharge [9]. Therefore, the majority of research reported from academia regarding LiS cells is based on electrolyte solvents containing ethers or respective derivatives [1]. Despite the well-known degradation in carbonate electrolyte-based LIB systems [10,11] and the reversible conversion of sulfur to lithium polysulfides [12–15], reports on the decomposition products emerging in electrolytes of LiS cells are rare. Schneider et al. analyzed the compositional changes of the electrolyte in LiS cells upon cycling and the evolution of H<sub>2</sub>, N<sub>2</sub>, CH<sub>4</sub> and C<sub>2</sub>H<sub>6</sub> by means of gas chromatography (GC) with flame ionization and thermal conductivity detectors [16]. However, this study did not include any degradation products besides the mentioned permanent gases. In the LIB context, electrolyte analyses by gas chromatography [10,16] and ion chromatography–conductivity detection (IC-CD) [17] have proven to be valuable tools to elucidate these phenomena. GC systems are suitable to separate volatile organic compounds such as ethers and carbonates; thus, the application of a combination with mass spectrometric (MS) systems is a promising technique to directly identify emerging compounds. Moreover, solid phase microextraction (SPME) can be used as a sampling technique for GC systems if there is not enough liquid electrolyte to be extracted from the cells without the use of extraction solvents. The method additionally benefits from the elimination of corrosive conductive salts such as LiPF<sub>6</sub> [18]. In order to adapt the developed methods for ether-based LiS electrolytes and their potential aging products, model experiments might be helpful. From the LIB context, different model aging experiments, such as thermal aging of single components and electrolyte formulations [17] or the introduction of reactive species [19], are well known. Besides the method development, which benefits from the abundance of larger sample amounts (milli-liter vs. micro-liter range), it is often possible to identify groups of aging products potentially formed in the cells. Thereby, the optimization of measurement parameters with regard to the detection of formerly identified groups is often possible.

The instability of carbonate-based electrolytes in LiS systems has been considered in a variety of studies in academia. As an outcome, different approaches resulting in operational cells, such as the introduction of sulfur into microporous carbon materials [20–22] or the utilization of metal sulfides, have been reported in literature [23–25]. The reactivity of the polysulfide species and their depletion in carbonate-based systems is known to be the reason for the rapid cell aging. In the case of cell setups employing metal sulfide CAMs not forming soluble polysulfides, cell aging should be caused by other detrimental reactions. The presented work reports on the identification of soluble and volatile aging products in ether- as well as carbonate-containing electrolytes from lithium-sulfur and lithium-metal sulfide batteries.

## 2. Materials and Methods

### 2.1. Chemicals and Materials

Dimethyl carbonate (DMC; 99.9%) and ethylene carbonate (EC; 99.9%) were purchased from Merck (Darmstadt, Germany). LiPF<sub>6</sub> (99.89%) was obtained from BASF (Ludwigshafen, Germany). Furthermore, 1,3-dioxolane (DOL) (99.8%), 1,2-dimethoxy ethane (DME; 99.5%), LiNO<sub>3</sub> (99.99%) and sulfur (99.98%) were bought from Sigma Aldrich (St. Louis, MO, USA). LiTFSI was obtained from TOB New Energy Technology (Xiamen, China). Helium (6.0) was purchased from Westfalen+ (Münster, Germany).

## 2.2. Model Aging Experiments

First, 2 mL of the single components and the different mixtures of ethers and conducting salt (1,3-dioxolane (DOL) and dimethoxyethane (DME)), a mixture of both ethers, and the electrolyte of interest— $1 \text{ mol L}^{-1}$  lithium bis(trifluoromethanesulfonyl)imide (LiTFSI) in DOL/DME (1:1)—were stored in stainless steel cylinders at elevated temperatures ( $60 \text{ }^\circ\text{C}$ ). Furthermore, the electrolyte formulation was stored in the same setup with the addition of elemental sulfur to mimic the environment in the cells and introduce the active material. The containers were tightly closed and stored at  $60 \text{ }^\circ\text{C}$  in an oven (Binder; Tuttlingen, Germany) for one month. Sampling was done once per week by opening the container in a dryroom and removing  $10 \text{ }\mu\text{L}$  of the liquid electrolyte.

## 2.3. LiS Cells

Three layered pouch cells with sulfurized poly(acrylonitrile) (SPAN)-based cathode active material (CAM) [26] versus lithium metal were investigated. The cathodes consisted of SPAN, vapor-grown carbon nanofibers (VGCF) or Ketjen black as a conductive additive (CA) and a mixture of carboxymethyl cellulose (CMC)/styrene-butadiene rubber (SBR) (2/1) used as a binder. The ratio of the components was CAM:CA:binder; 97.3:30:3 coated on aluminum foam current collectors (see Nara et al. [2]) The cells were shipped to MEET Battery Research Center after electrochemical aging (20 cycles at  $\sim 0.45 \text{ mA cm}^{-2}$  between 1.0 V and 3.0 V) performed by the authors from Waseda University. The applied electrolyte was  $1 \text{ mol L}^{-1}$  LiTFSI in DOL/DME (1:1; *v:v*).

For all following cells with standard LiS CAM, the lithium foil was roll-pressed from  $500 \text{ }\mu\text{m}$  to  $350 \text{ }\mu\text{m}$  according to Becking et al. [27]. Afterwards, disks of 12 mm diameter were punched and combined with Celgard2500 separators (Celgard; Charlotte, NC, USA) for the coin cell assembly. The cathode active material consisted of sulfur melt infiltrated into Ketjen black (C/S) mixed with multi-walled carbon nanotubes (Nanocyl MWCNT) and poly(tetrafluoroethylene) (PTFE) in a weight ratio of 90:7:3 (C/S:MWCNT:PTFE) to result in a sulfur content of 60 wt% in the final electrode (similar to Weller et al. [28]). Lithium-sulfur cells with  $60 \text{ }\mu\text{L}$  of ether-based electrolyte ( $0.25 \text{ mol L}^{-1}$   $\text{LiNO}_3$  and  $1 \text{ mol L}^{-1}$  LiTFSI in DOL/DME; 1:1; *w:w*) or carbonate-based electrolyte ( $1 \text{ mol L}^{-1}$   $\text{LiPF}_6$  in EC/DMC; 1:1; *w:w*) were built with 14 mm disks of standard LiS cathodes. The cells were cycled at  $0.66 \text{ mA cm}^{-2}$  for the first three cycles and at  $0.2 \text{ mA cm}^{-2}$  in a voltage window of 1.8 V to 2.6 V until 100 cycles were reached.

Cathodes with titanium sulfide as the active material (see Sakuda et al. [23]) were used in two-electrode coin cells with Celgard2500 separator (Celgard, Charlotte, NC, USA) and  $60 \text{ }\mu\text{L}$  of electrolyte ( $1 \text{ mol L}^{-1}$   $\text{LiPF}_6$  in DMC/EC; 1:1; *w:w*). The weight ratio of  $\text{TiS}_4$ , Ketjen Black (KB) and binder was 79:8:13. The cells were cycled in a voltage window of 1.9 V to 3.0 V, with  $0.02 \text{ mA cm}^{-2}$  for the first three cycles and at  $0.06 \text{ mA cm}^{-2}$  until 100 cycles were reached.

## 2.4. Cell Opening Procedure

All cells were opened in the fully charged state to minimize possible influences of remaining reactive polysulfide species. The cells were cut open in a glovebox, and separators and/or cathodes were transferred to Eppendorf vials and centrifuged with 17,000 rpm at  $20 \text{ }^\circ\text{C}$  in a cooled MEGA STAR 600R (VWR; Radnor, PA, USA) equipped with a fixed-angle HIGHConic rotor (Thermo Fisher Scientific; Waltham, MA, USA) to regain liquid electrolyte. For SPME measurements, a piece of the separator was transferred to a 20 mL headspace vial.

### 2.5. Analytical Measurements

The electrolyte was diluted by a factor of 1:100 in dichloromethane for GC measurements with liquid injection. For these measurements, 1  $\mu\text{L}$  of the diluted sample was injected into the GC system using a 10  $\mu\text{L}$  syringe.

All extractions by SPME were executed at room temperature to prevent further aging of the electrolytes by thermal decomposition during the sampling procedure. The SPME setup from CTC Analytics (Zwingen, Switzerland) controlled by the cycle composer software of the AOC 5000 autosampler (Shimadzu; Kyoto, Japan) was used. Acrylate with 85  $\mu\text{m}$  coatings were bought from Axel Semrau (Sprockhövel, Germany) and exposed to the headspace vial for an extraction time of 1 min or 10 min. After the measurement, the fiber was conditioned for 5 min at 260  $^{\circ}\text{C}$  under argon atmosphere (+50 kPa) in a needle heater unit.

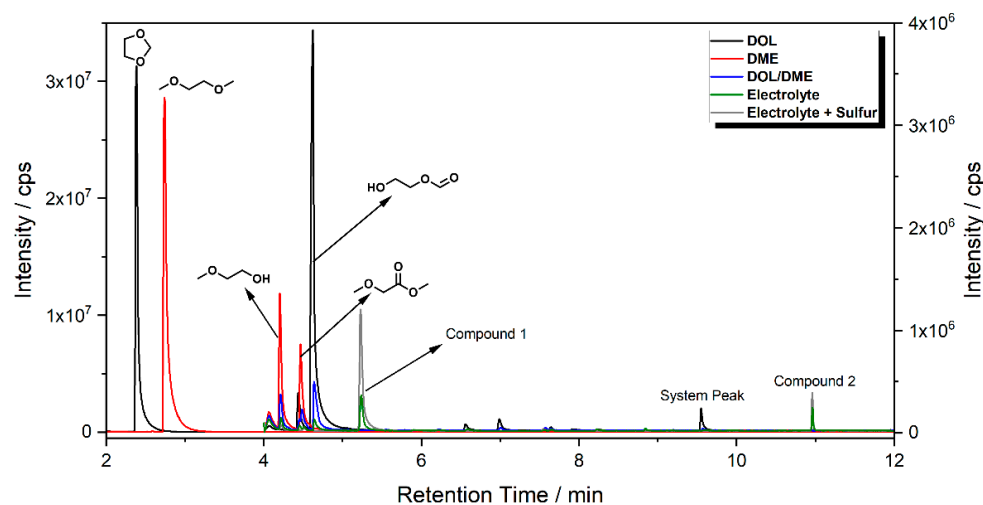
The GC-MS measurements were done with a GCMS-QP2010 Ultra equipped with an AOC 5000 Plus autosampler (both Shimadzu, Kyoto, Japan). A nonpolar Supelco SLB<sup>TM</sup>-5ms (30 m  $\times$  0.25 mm  $\times$  0.25  $\mu\text{m}$ , Sigma Aldrich; St. Louis, MO, USA) column was used. The system was controlled by the GCMS Real Time Analysis with implemented Cycle Composer for the AOC 5000 Plus autosampler (all Shimadzu; Kyoto, Japan). The obtained chromatograms were analyzed with GCMS Postrun Analysis (Shimadzu; Kyoto, Japan). Compounds were validated with the National Institute of Standards and Technology (Gaithersburg, MD, USA) NIST 11 library. DMC, EC, DOL, DME were additionally confirmed by the comparison of their retention times and fragment patterns with commercially available standards. Helium (6.0 purity) was used as a carrier gas with 1.16  $\text{mL min}^{-1}$  column flow and 3  $\text{mL min}^{-1}$  purge flow. The temperature program started at 40  $^{\circ}\text{C}$ , which was held for 1 min. Afterwards, temperature ramps with 3  $^{\circ}\text{C min}^{-1}$  until 60  $^{\circ}\text{C}$  and 30  $^{\circ}\text{C min}^{-1}$  until 260  $^{\circ}\text{C}$  followed. The final temperature was held for 2 min. The overall measurement time was 16.33 min, with a mass range of 20–350  $m/z$  and an event time of 0.2 s in scan mode. The mass spectrometer was run in electron ionization (EI) mode with the following parameters: the temperature of the ion source was set to 200  $^{\circ}\text{C}$ ; the interface was held at 250  $^{\circ}\text{C}$  and the filament was operated at a voltage of 70 V; the detector voltage was set relative to the respective tuning results.

Measurements with GC-HRMS were done on a GC QExactive (Thermo Fisher Scientific; Waltham, MA, USA) with the same nonpolar Supelco SLB<sup>TM</sup>-5ms (30 m  $\times$  0.25 mm  $\times$  0.25  $\mu\text{m}$ , Sigma Aldrich; St. Louis, MO, USA) column. All other parameters were applied as described by Peschel et al. [29].

## 3. Results and Discussion

### 3.1. Ether-Based Systems

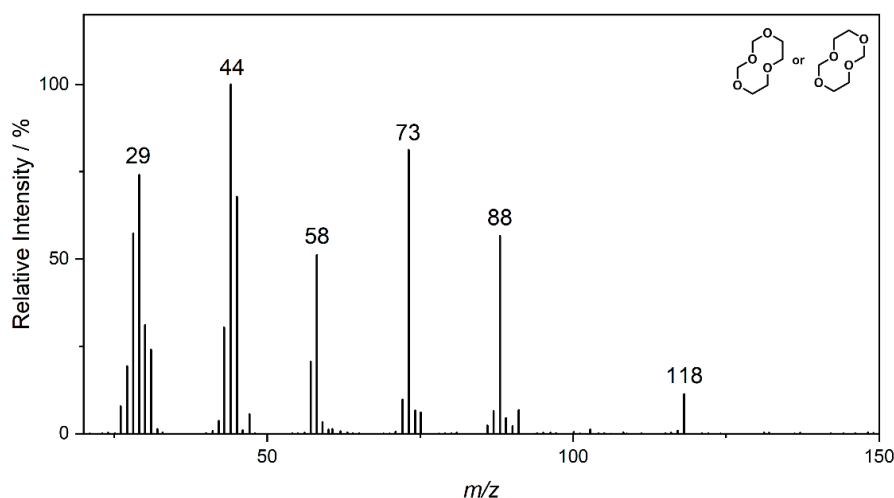
Model aging experiments by applying thermal stress or by the addition of trace water have proven to give viable information about possible aging mechanisms in lithium ion battery (LIB) electrolytes [10,17]. Furthermore, the transfer of analytical methods to new sample types—in this case, to LiS electrolytes—typically needs large sample amounts, as this is beneficial for both the method development and first insights into possible aging routes. To gain initial information about the behavior of ether-based formulations, the individual components' thermally induced aging phenomena were investigated. The chromatograms achieved by gas chromatography-mass spectrometry (GC-MS) are summarized in Figure 1. In general, the samples taken after the longest aging period (one month) showed the strongest signals of all the contained analytes; therefore, the results shown in the following paragraphs are all based on this sampling period.



**Figure 1.** Overlay of the GC-MS chromatograms obtained from ethers and ether-based electrolytes stored at elevated temperatures. Excerpt from 2–4 min extracted from measurements with 1:100 split ratio. Chromatograms from 4 min were obtained with a lower split ratio of 1:10.

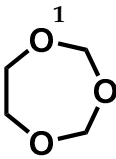
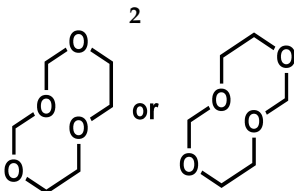
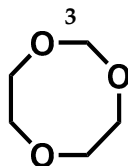
Both ether solvents are accessible by GC-MS and are the main components in all cases. However, several additional signals assigned to aging products that emerged during the storage time are present in the chromatograms. The samples of the single components show signals of small molecules identified by the NIST11 database. These compounds, which are connected, e.g., to the ring opening of DOL or the loss of a methyl group in the case of DME, show significantly lower responses in the mixture and are almost absent in the case of the complete electrolyte. Nevertheless, the chromatograms of the electrolyte samples show additional signals at later retention times. A direct identification was only possible for the compound eluting at 5.2 min (compound 1). In this case, the library comparison suggested an ether-based ring structure where a  $\text{CH}_2\text{O}$  group is added to the DOL. This suggestion is supported by experiments with chemical ionization (CI) and high-resolution mass spectrometry (HRMS). In the case of compound 2 eluting at 11 min, the library suggests an ether-based ring structure as well.

In this case, the fragment pattern shown in Figure 2 does not have a sufficient pendant in the NIST. Therefore, the samples were investigated thoroughly by GC-CI-MS and GC-HRMS. GC-CI-MS in positive mode revealed the molecular masses summarized in Table 1.



**Figure 2.** Fragment spectrum obtained by GC-MS of compound 2 eluting at 10.9 min and labeled as indicated in Figure 1. The  $m/z$  ratio of prominent fragments is given at the respective signals.

**Table 1.** Summary of the MS data from compounds of interest in DOL/DME-based systems. Parental fragments of compound 1 were too small to provide significant daughter ions in fragmentation experiments.

Compound			
Ret. Time	5.25 min	10.95 min	7.60 min
PCI	105 [M + H] <sup>+</sup> 122 [M + NH <sub>4</sub> ] <sup>+</sup>	149 [M + H] <sup>+</sup> 166 [M + NH <sub>4</sub> ] <sup>+</sup>	119 [M + H] <sup>+</sup> 136 [M + NH <sub>4</sub> ] <sup>+</sup>
NCI	73; 61	117	87
HRMS	105.0557 C <sub>4</sub> H <sub>9</sub> O <sub>3</sub> (5.0 ppm)	149.0814 C <sub>6</sub> H <sub>13</sub> O <sub>4</sub> (0.1 ppm)	119.0718 C <sub>5</sub> H <sub>11</sub> O <sub>3</sub> (8.2 ppm) 87.0456 (C <sub>4</sub> H <sub>7</sub> O <sub>2</sub> )
(HR)MS <sup>2</sup>	-	75.0446 (C <sub>3</sub> H <sub>7</sub> O <sub>2</sub> ) 45.0340 (C <sub>2</sub> H <sub>5</sub> O)	71.0503 (C <sub>4</sub> H <sub>7</sub> O) 59.0497 (C <sub>3</sub> H <sub>7</sub> O) 45.0339 (C <sub>2</sub> H <sub>5</sub> O)

The molecular mass of 148 u hints at a molecule containing two DOL moieties. This conclusion is supported by the HRMS experiments, which show a perfect fit for the suggested molecular formula and include one double bond equivalent. The fragmentation experiments cannot clarify the location of the CH<sub>2</sub>O vs. C<sub>2</sub>H<sub>4</sub>O groups, leading to two possible structural formulas, as summarized in Figure 2 and Table 1.

The GC-CI-MS and GC-HRMS experiments show an additional signal at 7.65 min (compound 3), which cannot be assigned from the GC-MS chromatogram. The experiments suggest a ring structure as with compound 1 with one additional CH<sub>2</sub> moiety. The analysis of the electrolyte regained from cycled standard LiS cells built with cathodes from TU Dresden and SPAN-based cells provided by Waseda University is shown in Figure 3. The corresponding cycling behavior is summarized in the supporting information (Figures S1 and S2). The overlay of the chromatograms shows that compounds 1 and 2 are present in the case of the SPAN cells, while the standard LiS cells show a matching signal of compound 2 with much higher intensity. This confirms the comparability of the model aging experiments and the aging of electrolytes in cells with sulfur-based CAM. The chromatogram from the SPAN cell contains additional small peaks. Since these peaks show only low intensities and the respective compounds are not formed in the model experiment, a structural elucidation could not be performed. The peak at 11.3 min in the LiS cell chromatogram is caused by column bleeding and does not originate from the sample.

A complementary investigation of the conductive salt by ion chromatography–conductivity detection (IC-CD) showed no additional signals; thus, the significant accumulation of ionic decomposition products can be excluded.

Model aging experiments showed the accumulation of higher-molecular circular ethers in DOL/DME-based electrolytes stored at high temperatures. The same aging products were identified in electrolytes regained from cells with different sulfur-based cathodes. Therefore, the developed analytical method as well as the model aging at elevated temperatures have proven to be valuable tools to investigate the aging behavior of LiS and related battery systems.

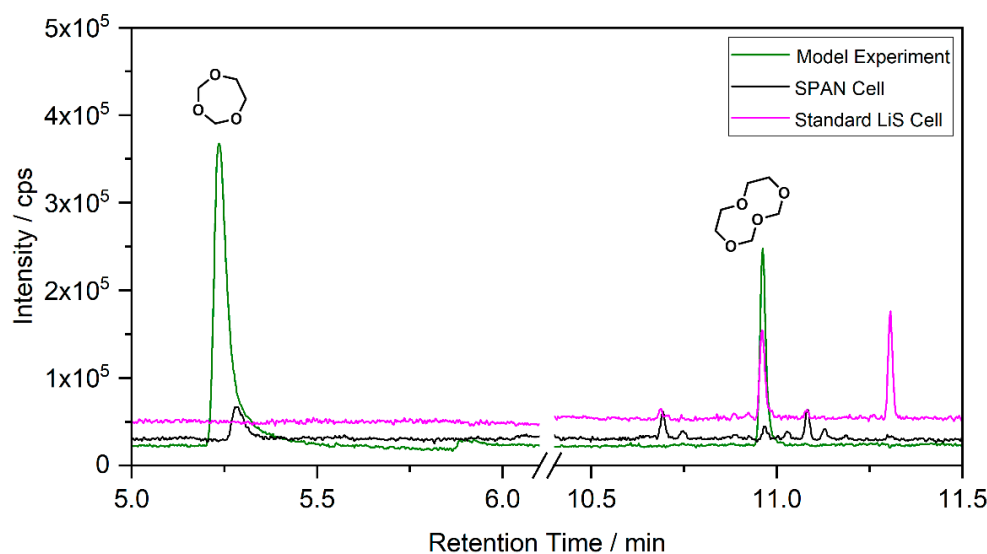
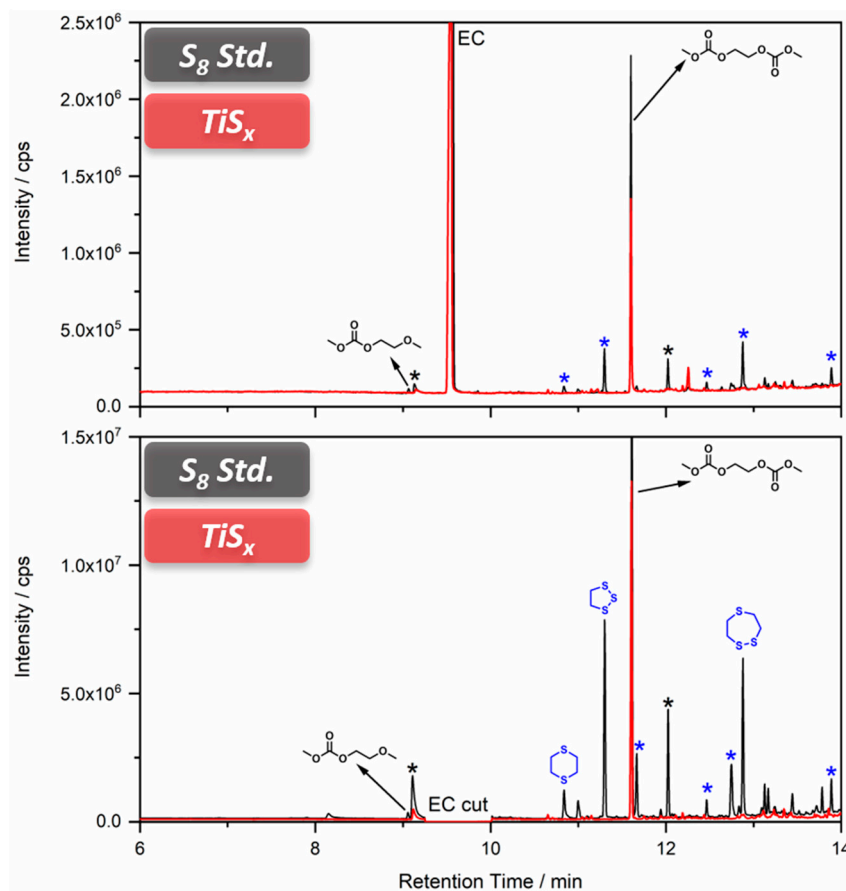


**Figure 3.** Chromatograms obtained by SPME–GC–MS from ether-based electrolytes used in LiS cell compared to the model experiment. Model experiment (green); SPAN cell with 1 mol/L LiTFSI in DOL/DME (black); standard LiS cell with additional LiNO<sub>3</sub> additive (0.25 mol/L; magenta).

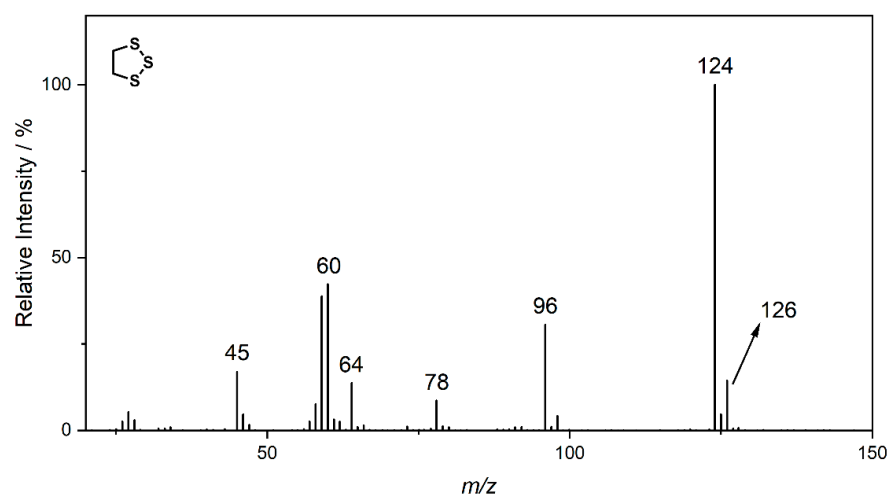
### 3.2. Carbonate-Based Systems

Since the general aging behavior of carbonate-based electrolytes is known from LIB research, the analytical method development is already reported. However, the presence of sulfur-based redox active species might introduce a new group of decomposition products, which would indicate a detrimental reaction of the electrolyte. After the determination of such species, it is possible to realize a target analysis of electrochemically aged electrolytes. Thus, the first experiments were done in expectation of high amounts of aging products (as a worst-case scenario) in combination with a non-target analysis. Therefore, a standard LiS cathode was cycled in a cell with an electrolyte comprising 1 mol L<sup>−1</sup> LiPF<sub>6</sub> in DMC/EC (1:1; *w/w*). These cells were not able to complete one full cycle and broke down immediately, as depicted in Figure S3. The electrolyte was investigated by GC–MS with liquid injection and SPME. The chromatogram (Figure 4) shows a mixture of decomposition products known from the LIB context and additional signals that are linked to the presence of sulfur.

The decomposition product with the highest signal intensity is the dimethyl-2,5-dioxahexane dicarboxylate (DMDOHC), which is reported to be the main product in EC/DMC-based electrolytes in LIBs [16]. However, there is a variety of signals present, which are not reported in the LIB context. The sulfur isotopes <sup>32</sup>S (95%) <sup>34</sup>S (4.3%) show typical mass shifts in the fragment patterns depending on the sulfur content of the respective molecular formula. Therefore, it is possible to distinguish between solely carbonate-based aging products and sulfur-containing derivatives even without the need of an HRMS system. Three of the most prominent sulfur-containing aging products were identified by the NIST11 database (Figure 4). The fragment pattern of the signal assigned to 1,2,3-trithiolane (compound B) is exemplarily shown in Figure 5.



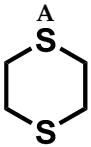
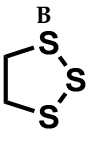
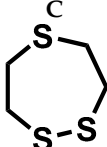
**Figure 4.** Overlay of the chromatograms obtained from carbonate-based electrolytes regained from sulfur-based cells. Measurements with 1:100 split ratio top and 1:10 bottom. Chromatograms connected to cells with standard sulfur cathodes are shown in black; titanium sulfide cells are depicted in red. Signals corresponding to aging products with carbonate origin are marked in black; aging products containing sulfur species are colored in blue. The structures of compounds with positive structural elucidation are shown at their respective signal. Signals without complete structural elucidation are marked with asterisks.



**Figure 5.** Fragment pattern of compound B eluting at a retention time of 11.25 min (Figure 4). The  $m/z$  ratio of prominent fragments is given at the respective signals. The fragment pattern is assigned to 1,2,3-trithiolane by the NIST11 database.

The signal at  $m/z$  124, which represents the  $M^+$  ion, shows the typical fragment at  $m/z$  125, which is connected to the  $^{13}\text{C}$  isotope. Moreover, the signal at  $m/z$  126, which is connected to the  $^{34}\text{S}$  isotope, is present at around 14.5% of the intensity of the main fragment. Since the intensity of the isotope fragment is proportional to the respective number of sulfur atoms in the ion, the presence of three sulfur atoms could be verified. Further HRMS experiments supported this assumption by adding the impact of the negative mass defect of the sulfur isotopes, providing distinct molecular formulas and daughter ions in  $\text{MS}^2$  experiments. A summary of the different compounds and corresponding fragments is shown in Table 2.

**Table 2.** Summary of the MS data from compounds of interest in carbonate-based systems.

Compound			
Ret. Time	10.84 min	11.30 min	12.88 min
MS	120; 60; 61	124; 96; 64; 60; 59	152; 124; 87; 64; 60; 59
NCI	below limit of detection	64	92
HRMS	120.0062 $\text{C}_4\text{H}_8\text{S}_2$ (4.5 ppm)	123.9470 $\text{C}_2\text{H}_4\text{S}_3$ (4.1 ppm)	151.9783 $\text{C}_4\text{H}_8\text{S}_3$ (3.4 ppm)
(HR)MS <sup>2</sup>	61.0106 ( $\text{C}_2\text{H}_5\text{S}$ ) 60.0027 ( $\text{C}_2\text{H}_4\text{S}$ )	95.9157 ( $\text{S}_3$ ) 63.9436 ( $\text{S}_2$ ) 58.9949 ( $\text{C}_2\text{H}_3\text{S}$ )	123.9470 ( $\text{C}_2\text{H}_4\text{S}_3$ ) 87.0263 ( $\text{C}_4\text{H}_7\text{S}$ ) 63.9436 ( $\text{S}_2$ ) 60.0028 ( $\text{C}_2\text{H}_4\text{S}$ )

The investigation of the electrolyte from electrochemically aged cells with titanium sulfide (Figure S4) as CAM reveals that the soluble electrolyte species are solely carbonate-based. No trace of sulfur-containing aging products was found, with DMDOHC being the main aging product. To exclude a similar but much slower aging behavior of the titanium sulfide cells in comparison to the standard LiS cells, characteristic fragments of the compounds of interest were defined ( $m/z$  60 ( $\text{C}_2\text{H}_4\text{S}$ ),  $m/z$  64 ( $\text{S}_2$ )). Thereby, it was possible to realize a target analysis besides the discussion of the total ion chromatogram (TIC).

Figure 6 shows the comparison of the TIC and the extracted ion chromatograms (EICs) of the characteristic fragments. Either both or at least one of the EICs shows a response for all signals of interest in the electrolyte cycled with standard LiS cathodes. This leads to the conclusion that the majority of sulfur-containing aging products can be targeted by using the two described fragments. However, the electrolyte from titanium sulfide cells shows no respective signals, although the EICs are strongly factorized. The sole signal for  $m/z$  60 at a retention time of 11.6 min corresponds to a fragment of DMDOHC including one  $^{13}\text{C}$  isotope. Therefore, the developed tailored electrolyte analysis was able to prove that the dissolution of sulfur-based species into the electrolyte and following side reactions with carbonates do not progress during cycling. Nevertheless, the cycle properties of the respective  $\text{TiS}_4$  cells (Figure S4) and especially the connected discharge capacity worsened with increasing cycle number. This means that there are deterioration factors other than the dissolution of sulfur, and the whole picture of the reaction mechanism of  $\text{TiS}_4$  would be clarified by analyzing the electrode surface as well. However, the aging products identified in the electrolyte are all known from analyses of LIBs, hinting at similar decomposition routes.

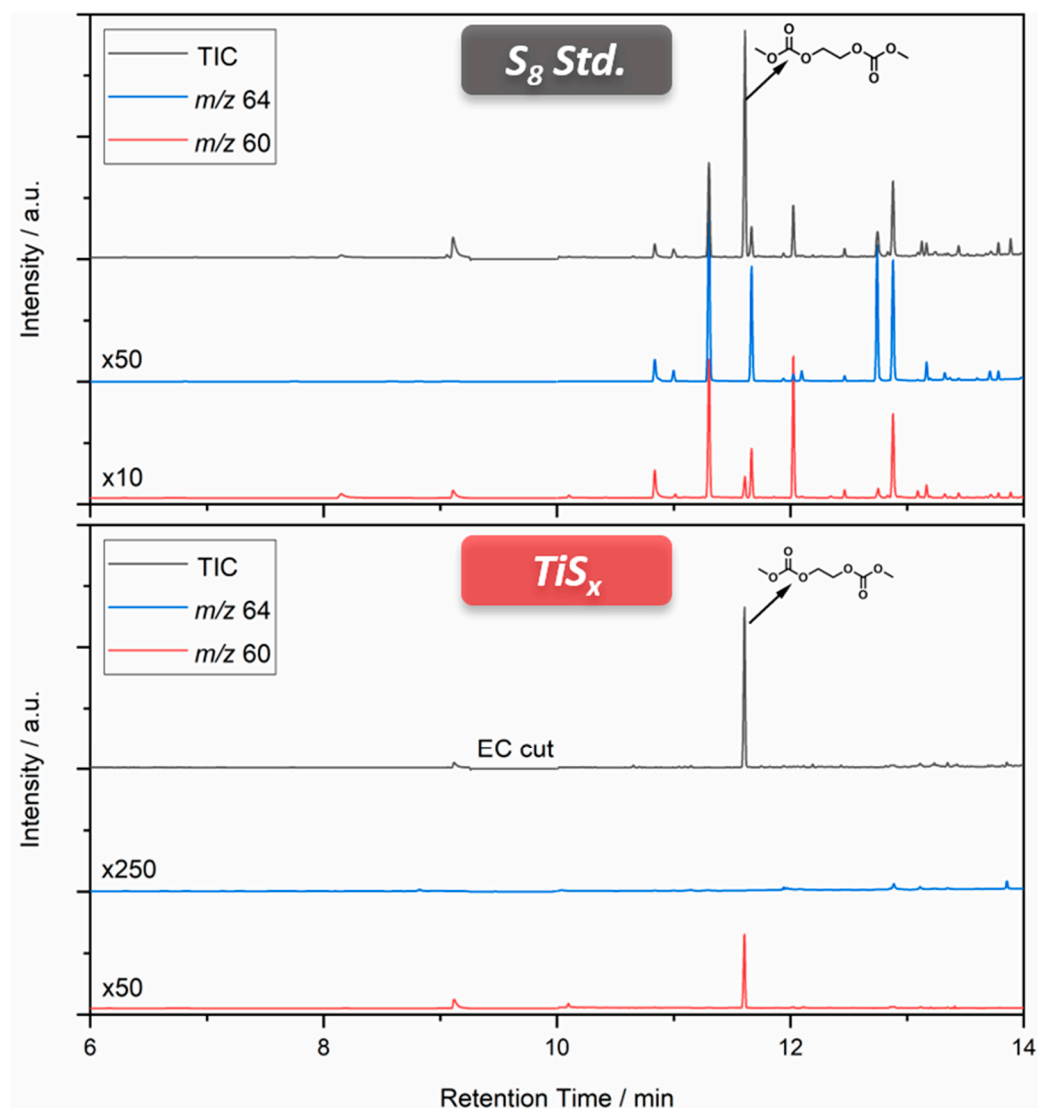


**Figure 6.** TICs and EICs connected to the carbonate-based electrolytes regained from cells with sulfur/titanium sulfide cathodes.

#### 4. Conclusions

The combination of model aging of ether-based electrolytes for LiS cells and a method transfer for GC-(HR)MS analyses of LIB electrolytes enabled the identification of thermally induced decomposition products. A subsequent analysis of electrolytes regained from LiS cells of different formats showed the applicability of the methods. Moreover, the identified, thermally induced ether polymerization was found in electrochemically aged cells as well, underlining the applicability of the respective model experiments for non-target analyses. The identified aging products showed that the reaction of DOL results in larger ring structures, representing an important aging mechanism.

In the context of carbonate-based electrolytes for model—worst-case—experiments with cells using standard LiS cathode materials, the results exhibited a variety of sulfur-containing compounds. The determination of characteristic fragments for these organosulfur compounds enabled target analyses for further samples. The electrolyte regained from operative cells with titanium sulfide as CAM did not show any signs of organosulfur compounds, while polymerization products of carbonates known from LIB research were present in typical amounts. In contrast to elemental sulfur as a cathode material that potentially leads to the severe formation of sulfur-containing species within the electrolyte, titanium sulfide does not cause any pronounced formation of soluble electrolyte degra-

dation products beyond the ones already known from LIB chemistries. Therefore, the presented method is fit for the purpose of investigating carbonate-based electrolytes from other cell chemistries. Within this context, the determination of the main reaction mechanisms of cathodes using sulfur encapsulation in microporous structures and carbonate electrolytes is of special interest. The determination of decomposition routes can then be used to backtrack important reactivities and suggest improvements for the next generation of cathode materials.

**Supplementary Materials:** The following supporting information can be downloaded at: <https://www.mdpi.com/article/10.3390/separations9030057/s1>, Figure S1: Cell voltage versus capacity plots of different charge/discharge cycles from a standard LiS cell with ether-based electrolyte; Figure S2: Cell voltage versus specific capacity (mass of sulfur) plots of different charge/discharge cycles of a cell with SPAN as active material on an aluminum foam current collector. VGCF was used as conductive additive and the electrolyte was ether-based. Figure S3: Cell voltage versus capacity plot of a cell built with standard LiS cathodes and carbonate-based electrolyte. Figure S4: Cell voltage versus capacity plots of charge/discharge cycles of a cell with TiS<sub>4</sub> as active material and carbonate-based electrolyte.

**Author Contributions:** F.H., investigation, writing—original draft; C.P., investigation; K.K. (Kristina Kösters), investigation; S.N., supervision; K.K. (Kentaro Kuratani), investigation; T.T., investigation; H.M., investigation; F.S., investigation; H.S., supervision; S.K., supervision; T.O., supervision; M.W., writing—review and editing; H.N., writing—review and editing; S.W.-M., supervision, validation. All authors have read and agreed to the published version of the manuscript.

**Funding:** The authors thank the German Federal Ministry of Education and Research for funding the project AReLiS (03XP0229A).

**Institutional Review Board Statement:** Not applicable.

**Informed Consent Statement:** Not applicable.

**Data Availability Statement:** Data are available upon reasonable request from the corresponding authors.

**Conflicts of Interest:** The authors declare no conflict of interest. The funders had no role in the design of the study; in the collection, analyses, or interpretation of data; in the writing of the manuscript, or in the decision to publish the results.

## References

1. Zhang, S.S. Liquid electrolyte lithium/sulfur battery: Fundamental chemistry, problems, and solutions. *J. Power Sources* **2013**, *231*, 153–162. [[CrossRef](#)]
2. Nara, H.; Yokoshima, T.; Mikuriya, H.; Tsuda, S.; Momma, T.; Osaka, T. The Potential for the Creation of a High Areal Capacity Lithium-Sulfur Battery Using a Metal Foam Current Collector. *J. Electrochem. Soc.* **2017**, *164*, A5026–A5030. [[CrossRef](#)]
3. Placke, T.; Kloepsch, R.; Dühnen, S.; Winter, M. Lithium ion, lithium metal, and alternative rechargeable battery technologies: The odyssey for high energy density. *J. Solid State Electrochem.* **2017**, *21*, 1939–1964. [[CrossRef](#)]
4. Schmich, R.; Wagner, R.; Höpkel, G.; Placke, T.; Winter, M. Performance and cost of materials for lithium-based rechargeable automotive batteries. *Nat. Energy* **2018**, *3*, 267–278. [[CrossRef](#)]
5. Mikhaylik, Y.V.; Kovalev, I.; Schock, R.; Kumaresan, K.; Xu, J.; Affinito, J. High Energy Rechargeable Li-S Cells for EV Application: Status, Remaining Problems and Solutions. *ECS Trans.* **2010**, *25*, 23–34. [[CrossRef](#)]
6. Dörfler, S.; Althues, H.; Härtel, P.; Abendroth, T.; Schumm, B.; Kaskel, S. Challenges and Key Parameters of Lithium-Sulfur Batteries on Pouch Cell Level. *Joule* **2020**, *4*, 539–554. [[CrossRef](#)]
7. Dühnen, S.; Betz, J.; Kolek, M.; Schmich, R.; Winter, M.; Placke, T. Toward Green Battery Cells: Perspective on Materials and Technologies. *Small Methods* **2020**, *4*, 2000039. [[CrossRef](#)]
8. Xu, K. Nonaqueous Liquid Electrolytes for Lithium-Based Rechargeable Batteries. *Chem. Rev.* **2004**, *104*, 4303–4418. [[CrossRef](#)]
9. Manthiram, A.; Fu, Y.; Chung, S.-H.; Zu, C.; Su, Y.-S. Rechargeable Lithium-Sulfur Batteries. *Chem. Rev.* **2014**, *114*, 11751–11787. [[CrossRef](#)]
10. Gachot, G.; Ribière, P.; Mathiron, D.; Grugeon, S.; Armand, M.; Leriche, J.-B.; Pilard, S.; Laruelle, S. Gas Chromatography/Mass Spectrometry As a Suitable Tool for the Li-Ion Battery Electrolyte Degradation Mechanisms Study. *Anal. Chem.* **2011**, *83*, 478–485. [[CrossRef](#)]
11. Henschel, J.; Peschel, C.; Klein, S.; Horsthemke, F.; Winter, M.; Nowak, S. Clarification of Decomposition Pathways in a State-of-the-Art Lithium Ion Battery Electrolyte through C-13-Labeling of Electrolyte Components. *Angew. Chem. Int. Edit.* **2020**, *59*, 6128–6137. [[CrossRef](#)]

12. Barchasz, C.; Molton, F.; Duboc, C.; Leprêtre, J.-C.; Patoux, S.; Alloin, F. Lithium/Sulfur Cell Discharge Mechanism: An Original Approach for Intermediate Species Identification. *Anal. Chem.* **2012**, *84*, 3973–3980. [[CrossRef](#)]
13. Diao, Y.; Xie, K.; Xiong, S.Z.; Hong, X.B. Analysis of Polysulfide Dissolved in Electrolyte in Discharge-Charge Process of Li-S Battery. *J. Electrochem. Soc.* **2012**, *159*, A421–A425. [[CrossRef](#)]
14. Hagen, M.; Schiffels, P.; Hammer, M.; Dorfler, S.; Tubke, J.; Hoffmann, M.J.; Althues, H.; Kaskel, S. In-Situ Raman Investigation of Polysulfide Formation in Li-S Cells. *J. Electrochem. Soc.* **2013**, *160*, A1205–A1214. [[CrossRef](#)]
15. Patel, M.U.M.; Demir-Cakan, R.; Morcrette, M.; Tarascon, J.M.; Gaberscek, M.; Dominko, R. Li-S Battery Analyzed by UV/Vis in Operando Mode. *Chemsuschem* **2013**, *6*, 1177–1181. [[CrossRef](#)]
16. Schneider, H.; Weiß, T.; Scordilis-Kelley, C.; Maeyer, J.; Leitner, K.; Peng, H.-J.; Schmidt, R.; Tomforde, J. Electrolyte decomposition and gas evolution in a lithium-sulfur cell upon long-term cycling. *Electrochim. Acta* **2017**, *243*, 26–32. [[CrossRef](#)]
17. Kraft, V.; Grutzke, M.; Weber, W.; Winter, M.; Nowak, S. Ion chromatography electrospray ionization mass spectrometry method development and investigation of lithium hexafluorophosphate-based organic electrolytes and their thermal decomposition products. *J. Chrom. A* **2014**, *1354*, 92–100. [[CrossRef](#)]
18. Horsthemke, F.; Friesen, A.; Mönnighoff, X.; Stenzel, Y.P.; Grütze, M.; Andersson, J.T.; Winter, M.; Nowak, S. Fast screening method to characterize lithium ion battery electrolytes by means of solid phase microextraction—Gas chromatography—Mass spectrometry. *RSC Adv.* **2017**, *7*, 46989–46998. [[CrossRef](#)]
19. Gachot, G.; Grugeon, S.; Eshetu, G.G.; Mathiron, D.; Ribière, P.; Armand, M.; Laruelle, S. Thermal behaviour of the lithiated-graphite/electrolyte interface through GC/MS analysis. *Electrochim. Acta* **2012**, *83*, 402–409. [[CrossRef](#)]
20. Hippauf, F.; Nickel, W.; Hao, G.-P.; Schwedtmann, K.; Giebeler, L.; Oswald, S.; Borchardt, L.; Doerfler, S.; Weigand, J.J.; Kaskel, S. The Importance of Pore Size and Surface Polarity for Polysulfide Adsorption in Lithium Sulfur Batteries. *Adv. Mater. Interfaces* **2016**, *3*, 1600508. [[CrossRef](#)]
21. Li, S.; Fan, Z. Encapsulation methods of sulfur particles for lithium-sulfur batteries: A review. *Energy Storage Mater.* **2021**, *34*, 107–127. [[CrossRef](#)]
22. Li, S.; Leng, D.; Li, W.; Qie, L.; Dong, Z.; Cheng, Z.; Fan, Z. Recent progress in developing Li<sub>2</sub>S cathodes for Li-S batteries. *Energy Storage Mater.* **2020**, *27*, 279–296. [[CrossRef](#)]
23. Sakuda, A.; Takeuchi, T.; Okamura, K.; Kobayashi, H.; Sakaebe, H.; Tatsumi, K.; Ogumi, Z. Rock-salt-type lithium metal sulphides as novel positive-electrode materials. *Sci. Rep.* **2014**, *4*, 4883. [[CrossRef](#)] [[PubMed](#)]
24. Senoh, H.; Kageyama, H.; Takeuchi, T.; Nakanishi, K.; Ohta, T.; Sakaebe, H.; Yao, M.; Sakai, T.; Yasuda, K. Gallium (III) sulfide as an active material in lithium secondary batteries. *J. Power Sources* **2011**, *196*, 5631–5636. [[CrossRef](#)]
25. Balach, J.; Jaumann, T.; Giebeler, L. Nanosized Li<sub>2</sub>S-based cathodes derived from MoS<sub>2</sub> for high-energy density Li-S cells and Si-Li<sub>2</sub>S full cells in carbonate-based electrolyte. *Energy Storage Mater.* **2017**, *8*, 209–216. [[CrossRef](#)]
26. Wang, W.; Cao, Z.; Elia, G.A.; Wu, Y.; Wahyudi, W.; Abou-Hamad, E.; Emwas, A.-H.; Cavallo, L.; Li, L.-J.; Ming, J. Recognizing the Mechanism of Sulfurized Polyacrylonitrile Cathode Materials for Li-S Batteries and beyond in Al-S Batteries. *ACS Energy Lett.* **2018**, *3*, 2899–2907. [[CrossRef](#)]
27. Becking, J.; Gröbmeyer, A.; Kolek, M.; Rodehorst, U.; Schulze, S.; Winter, M.; Bieker, P.; Stan, M.C. Lithium-Metal Foil Surface Modification: An Effective Method to Improve the Cycling Performance of Lithium-Metal Batteries. *Adv. Mater. Interfaces* **2017**, *4*, 1700166. [[CrossRef](#)]
28. Weller, C.; Pampel, J.; Dörfler, S.; Althues, H.; Kaskel, S. Polysulfide Shuttle Suppression by Electrolytes with Low-Density for High-Energy Lithium-Sulfur Batteries. *Energy Technol.* **2019**, *7*, 1900625. [[CrossRef](#)]
29. Peschel, C.; Horsthemke, F.; Winter, M.; Nowak, S. Implementation of Orbitrap Mass Spectrometry for Improved GC-MS Target Analysis in Lithium Ion Battery Electrolytes. *MethodsX* **2022**, *9*, 101621. [[CrossRef](#)]